Mapping of the prostate in endorectal coil-based MRI/MRSI and CT: A deformable registration and validation study

J. Lian,[a] L. Xing,[b] and S. Hunjan
Department of Radiation Oncology, Stanford University School of Medicine, 875 Blake Wilbur Drive, Stanford, California 94305

C. Dumoulin
GE Corporate Research and Development Center, Schenectady, New York 12309

J. Levin
Department of Radiology, Stanford University School of Medicine, 875 Blake Wilbur Drive, Stanford, California 94305

A. Lo
Department of Radiation Oncology, Stanford University School of Medicine, 875 Blake Wilbur Drive, Stanford, California 94305

R. Watkins, K. Rohling, and R. Giaquinto
GE Corporate Research and Development Center, Schenectady, New York 12309

D. Kim, D. Spielman, and B. Daniel
Department of Radiology, Stanford University School of Medicine, 875 Blake Wilbur Drive, Stanford, California 94305

(Received 1 June 2004; revised 26 July 2004; accepted for publication 24 August 2004; published 28 October 2004)

The endorectal coil is being increasingly used in magnetic resonance imaging (MRI) and MR spectroscopic imaging (MRSI) to obtain anatomic and metabolic images of the prostate with high signal-to-noise ratio (SNR). In practice, however, the use of endorectal probe inevitably distorts the prostate and other soft tissue organs, making the analysis and the use of the acquired image data in treatment planning difficult. The purpose of this work is to develop a deformable image registration algorithm to map the MRI/MRSI information obtained using an endorectal probe onto CT images and to verify the accuracy of the registration by phantom and patient studies. A mapping procedure involved using a thin plate spline (TPS) transformation was implemented to establish voxel-to-voxel correspondence between a *reference* image and a *floating* image with deformation. An elastic phantom with a number of implanted fiducial markers was designed for the validation of the quality of the registration. Radiographic images of the phantom were obtained before and after a series of intentionally introduced distortions. After mapping the distorted phantom to the original one, the displacements of the implanted markers were measured with respect to their ideal positions and the mean error was calculated. In patient studies, CT images of three prostate patients were acquired, followed by 3 Tesla (3 T) MR images with a rigid endorectal coil. Registration quality was estimated by the centroid position displacement and image coincidence index (CI). Phantom and patient studies show that TPS-based registration has achieved significantly higher accuracy than the previously reported method based on a rigid-body transformation and scaling. The technique should be useful to map the MR spectroscopic dataset acquired with ER probe onto the treatment planning CT dataset to guide radiotherapy planning. [DOI: 10.1118/1.1806292]

I. INTRODUCTION

The introduction of endorectal (ER) surface coils significantly improves the spatial resolution and signal-to-noise ratio (SNR) of prostate MR and MR spectroscopic imaging.[1–8] The new MRI/MRSI tool provides an unprecedented means for us to characterize the location(s) and volume(s) of intraprostatic lesion(s) and to evaluate the possible capsular penetration, invasion of neurovascular bundle, and seminal vesicle involvement.[2–4,9–13] The information derived from the new imaging modality is also valuable for guiding radiation treatment planning to escalate radiation doses according to the regional tumor burden.[14–18] In practice, the use of an ER coil severely distorts the prostate and surrounding organs. On the other hand, current radiation treatment planning is performed on the CT images without distortion. CT has high geometric accuracy and provides valuable electron density information needed for accurate dose calculation. In order to use ER-based image data to guide radiation treatment planning, it is imperative to develop a method to map the information in the ER-based MRI/MRSI to the corresponding location in CT images.[19,20] Zaider *et al.*[17] and Mizowaki *et al.*[21] have reported a translation and scaling based registration method to map MRS positive volumes onto the CT and ultrasound images. In their approach, the coordinates of

the boundary and the center of mass were used to linearly interpolate the positions of the mapped voxels. Although a clinically acceptable mean difference (2.4 mm) between the predicted and measured positions was reported, larger discrepancy was found for regions with more severe distortion ($\geqslant$4 mm).

In order to fully use the functional data to guide radiation treatment planning, a mapping method with computation efficiency and acceptable accuracy is needed. The purpose of this paper is to present a thin plate spline (TPS)-based deformable registration to improve the previously reported nondeformable MRS and CT mapping technique and test the registration accuracy using a series of phantom measurements. The TPS transformation is a well-established mathematical method and its central idea is to find a continuous transformation to minimize the difference between the control points in two images. Since its first introduction into medical image analysis,[26] the TPS has been successfully used on several applications. A two step registration scheme (rigid body registration and TPS warping) was employed to make comparisons of MR images in interventional MRI guided radiofrequency ablation to determine whether a tumor is adequately treated.[22,23] In order to map changes in the shape and position of the liver between inhale and exhale breath held CT models of a patient, a mutual information (MI) based alignment with TPS warping was proposed.[24] A TPS transformation based technique has also been found useful to correct image distortion in fluoroscopic images.[25] We believe this method is a good tradeoff between computation complexity and registration accuracy and should be well suited in mapping deformed voxels of MRS onto CT image.

II. METHODS AND MATERIALS

A. Phantom construction and imaging

Tissue equivalent bolus material was used to construct the 2D phantoms which simulate the axial sections of the patient dataset. The bolus, made of vinyl gel, is elastic and has a density close to that of water. Ten to fifteen metal fiducial landmarks were embedded into each phantom. The phantoms were held in a custom made plastic holder, allowing them to be constricted and deformed in specifically chosen regions (Fig. 1). The radiographic images were then acquired in anterior-posterior (AP) and lateral (LT) direction using a Ximatron Radiotherapy Simulator (Varian Medical Systems, Palo Alto, CA). An analysis of the AP/LT images for each phantom revealed the geometric locations of the fiducial markers before and after the distortion.

B. Patient image acquisition

Patient MRI was acquired on a 3-Tesla MR scanner (Signa; GE Medical Systems, Milwaukee, WI). RF excitation was achieved by using the whole body birdcage resonator, and the MR signal was received using a 4-element phased-array antenna (G.E. Medical Systems, Milwaukee, WI) combined with a rigid single loop receiver-only surface coil with a fixed geometry that enables optimal tuning and matching for use at 3 T. The coil dimensions are similar to transrectal ultrasound transducers used for routine sonographically-guided prostate imaging and biopsy. The ER-induced distortion of MRSI is very close to that of MRI. We show MR images in this study because they have higher image quality than MRSI. MR images were acquired using axial fast spin echo TR/TE:6000/80.5 ms, echo train length: 48 ms, FOV: 10 cm, Matrix: 512×256 and Resolution: 195×390 μm. Patient CT images were acquired using a PQ5000 CT Scanner (Philips Medical Systems, Cleveland, OH). Three patients were recruited for the scanning. They have stage T1/T2 disease and pretreatment prostate specific antigen (PSA) level was $\leqslant$10 ng/ml.

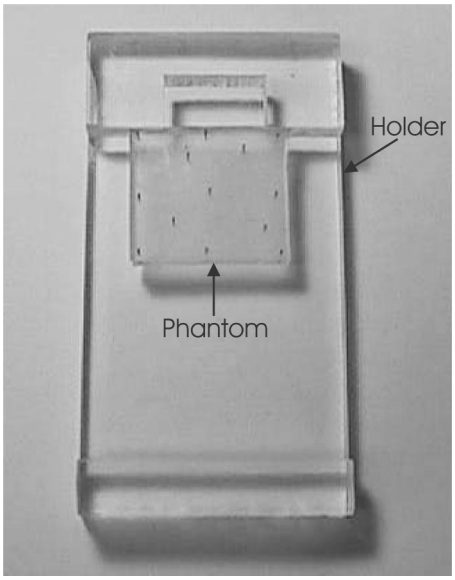

FIG. 1. A photo of the deformable phantom with implanted landmarks in a holder. The landmarks are used to calculate the registration error.

C. Image mapping method

After the acquisition of CT and MRS/MR image, the prostate volumes were contoured by an experienced oncologist. The rotation operator was applied to adjust the relative tilt between two volumes. The axial slices of CT and MR data set were resampled using 1 mm interval. We aligned CT and MR slices with reference to the apex and base of the glands. Four to eight control points were placed in each pair of slices. The control points were only put along the contour of the gland and they are featured points such as corners and intersections of edges. Lastly the TPS transformation was applied on each pair of slices to establish a mapping relationship between voxels of MRI and CT. For convenience, henceforth, the nondistorted CT volume is referred to as the *reference* and the distorted MRI the *floating* dataset.

The detailed description of the TPS transformation can be found in Bookstein's paper.[26] In brief, weighting vector $W=(w_1,w_2,\ldots,w_n)$ and the coefficients a_1, a_u, a_v are computed from a series of matrices which are constructed using n pairs of selected control points in the *reference* image (x_i,y_i)

and in the *floating* image (u_i, v_i). The function transforming a voxel in the *floating* volume to a new coordinate in the *reference* volume is defined as

$$f(u',v') = a_1 + a_u u + a_v v + \sum_{i=0}^{n} w_i U(|P_i - (u,v)|),$$

where P is the matrix of the coordinates of control points in the reference image and U is a basis function to measure the distance. The computation of the TPS transformation is rather efficient. In our experiment, it took around 5 s to compute a 520×520-pixel, 8-control point transformation on a Personal Computer (PC) with Intel Pentium® II 400 MHz CPU (Intel Corporation, Sunnyvale, CA) and 256 MB memory.

For comparison purposes, we also implemented the nondeformable registration method reported by Zaider *et al.*[17] and Mizowaki *et al.*[21] For a particular voxel in the MR space (coordinate z_1), the z coordinate in the US/CT space was obtained from

$$\frac{z_1 - z_{C_1}}{z_{T_1} - z_{B_1}} = \frac{z_2 - z_{C_2}}{z_{T_2} - z_{B_2}},$$

where z_{T_1} and z_{T_2} are the coordinates of the superior aspects of the prostate in the MR and US/CT volume, respectively, z_{B_1} and z_{B_2} refer to the z coordinates of the inferior aspects of the prostate, respectively, and z_{C_1} and z_{C_2} represent the z coordinates of the prostate centroid in the MR space and US/CT space, respectively. Similarly, the (x,y) coordinates were mapped as follows:

$$\frac{y_{A_1} - y_{P_1}}{y_{A_1} - y_1} = \frac{y_{A_2} - y_{P_2}}{y_{A_2} - y_2},$$

$$\frac{x_{L_1} - x_{R_1}}{x_{L_1} - x_1} = \frac{x_{L_2} - x_{R_2}}{x_{L_2} - x_2}.$$

Here, y_A and y_P are the y coordinates of the anterior and posterior aspects of the prostate, respectively, and x_L and x_R refer to, respectively, the x coordinates of the left and right aspects of the prostate. The results obtained by using this method and the newly developed TPS method were quantitatively compared in the phantom and patient studies.

D. Validation of the image registration

For phantom studies, the control points were chosen only in the periphery for the registration of the *floating* and *reference* images. The inserted landmarks were used to trace the displacement and verify the registration accuracy. The control points used in the registration were excluded in computing registration error. After mapping the distorted phantom to the original one, the displacements of the implanted markers were measured with respect to their ideal positions and the mean discrepancy was calculated for each phantom. The mean landmark displacement error (MLDE) was used as a metric for evaluating the quality of the registration.

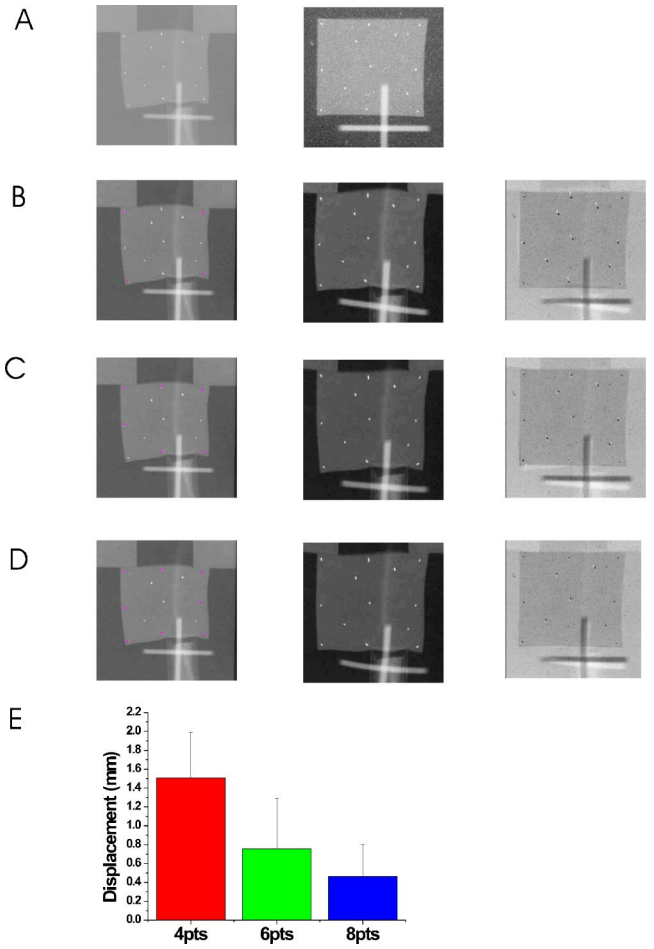

FIG. 2. A registration study using a square phantom deformed by external force. (A) The phantom under the influence of a force (left) and its original shape (right). The distorted phantom is shown in a smaller scale than the original phantom in order to include part of the holder and external object. (B) The position of four control points on the distorted phantom is indicated by pink plus signs (left). The middle shows the computed deformed image. The right column shows the difference image between the computer transformed image and original one. (C) and (D) are similar to B except that six and eight control points are used, respectively. (E) The landmark displacement of the three groups.

For patient studies, typically 6–8 control points were chosen along the contour of the prostate based on the pronounced feature in geometry. Patient MR and CT registration accuracy was estimated by using the centroid position displacement of the prostate and the coincidence index (CI) defined by

$$\mathrm{CI}(R,\mathrm{DF}) = \frac{\mathrm{DF} \cap R}{\mathrm{DF} \cup R},$$

where CI is unity when two structures overlap exactly and zero when they are completely disjoined.[27] The *deformed floating* (DF) image and the *reference* (R) images were converted to binary for the calculation. The intensity of the voxels inside the contour of the prostate was set 1 and that of other voxels was set 0. The use of CI provided us with an effective measure of the similarity between the warped

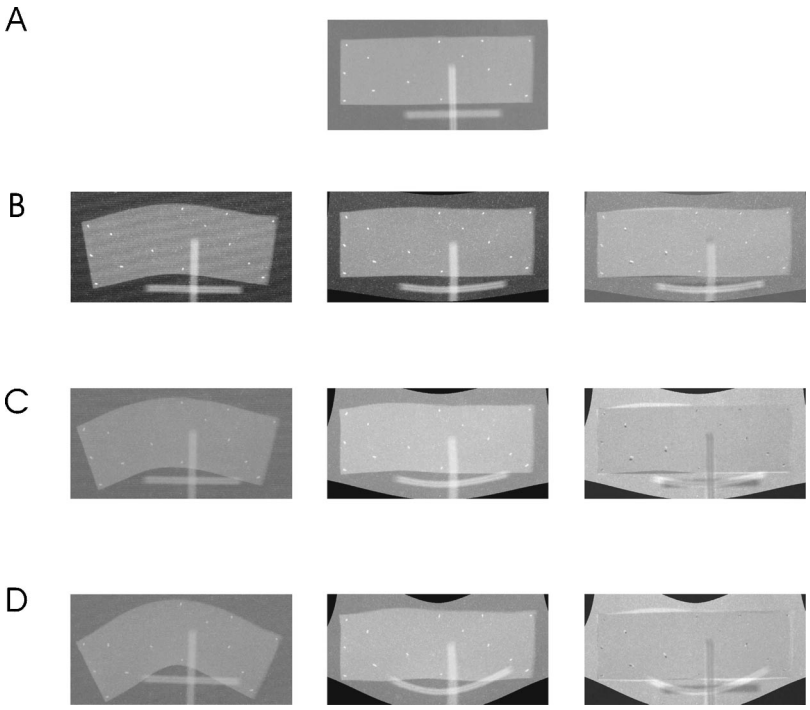

FIG. 3. A registration study by systematically bending a rectangular phantom. (A) The original phantom. (B) The distorted phantom (left), the TPS-warped phantom (middle) and the difference image between computed and original one (right). (C) and (D) are similar to (B) except with increased distortions.

floating (F) image and the *reference* (R) image. In both evaluations the tissue density was assumed to be homogeneous.

III. RESULTS

A. Phantom studies

We first studied the dependence of registration accuracy on the number of control points. An elastic phantom with dimension $5.5\times5.5\times1$ cm^3 was used here. The phantom was distorted by the insertion of an object in the holder [Fig. 2(A) left] and it restored to the original shape when the object was removed [Fig. 2(A) right]. When four control points were selected along the margin [Fig. 2(B) left], we obtained the warped image shown in the middle column. To evaluate the TPS algorithm, we computed the difference between the TPS predicted and the true image [Fig. 2(B) right panel]. The MLDE was found to be 1.51 ± 0.49 mm. It is seen that the implanted landmarks do not coincide well in the two images. Next we added two more control points in the periphery and the corresponding mapped image shows reduced registration error with MLDE down to 0.76 ± 0.54 mm [Fig. 2(C)]. When eight control points were selected, the MLDE was further reduced to 0.46 ± 0.34 mm and no significant landmark displacement was found in the difference image [Fig. 2(D)]. In Fig. 2(E) we summarized the MLDEs when four, six and eight control points were used in the warping calculation. The use of more control points resulted in higher registration accuracy. In practice, however, increasing the number of control points requires additional manual interaction and prolongs the registration process. In the following studies, six to eight pairs of control points were selected for the TPS registration. We also mapped the distorted phantoms onto the *reference* images using a rigid-body registration and scaling based method.[17,21] The nondeformable registration resulted in a 2.50 ± 0.83 mm MLDE when the maximum displacement was 4.2 mm. Hence, in the situation of a 4.2 mm distortions, the TPS method with eight control points yielded a MLDE that was only 18.4% of the MLDE obtained with the nondeformable model (0.46 vs 2.50 mm).

In the next level of validation we tested the algorithm with a larger rectangular phantom ($9.2\times5.1\times1$ cm) to allow more flexible distortions. The *reference* image is shown in Fig. 3(A). The *floating* images under a few different levels of distortion are shown in the left columns of B, C, and D. Eight control points were used here to register the *floating* and *reference* images. The middle panels of B, C, and D show the results after the TPS transformation. The differences between the TPS predictions and *references* are shown on the right panels of B, C, and D. The quality of the TPS mapping was assessed by using the maximum and mean landmark displacement error. As summarized in Table I, for the distortion shown in Fig. 3(A), the nondeformable registration gave a MLDE of 4.62 ± 2.71 mm, whereas the deformable registration reduced the error down to 0.45 ± 0.53 mm. For the studies shown in Figs. 3(C) and 3(D), the nondeformable registration yielded MLDEs to 7.35 ± 4.20 mm and 12.95 ± 6.57 mm, respectively. The maximum displacement errors in some fiducials are larger than 10 mm. The application of the deformable warping module significantly improved the mapping and led to MLDEs of 0.57 ± 0.49 mm and 0.62 ± 0.39 mm, respectively. The total displacements of control points to bring about the registration are 38.43, 58.76, and 102.34 mm, respectively, in these cases (Table I). The registration errors increase with them. The largest registration error between the TPS prediction and the ideal situation were found to be 1.09 mm, 1.05 mm, and 0.99 mm, respectively, for the three phantom distortions.

TABLE I. Deformable and nondeformable registration error of the distorted phantoms shown in Figs. 3(B)–3(D). Total displacements of control points (CPs) to bring about the registration are listed. The maximum refers to the maximum landmark displacement error and the mean refers to the mean landmark displacement error in each case.

Distortion (mm)	Total displacements of CPs	Nondeformable registration		Deformable registration	
		Maximum	Mean	Maximum	Mean
Fig. 3(B)	38.43	9.83	4.62±2.71	1.09	0.45±0.53
Fig. 3(C)	58.76	14.74	7.35±4.20	1.05	0.57±0.49
Fig. 3(D)	102.34	23.07	12.95±6.57	0.99	0.62±0.39

Considering the severity of the distortion in this example and the voxel size of MRSI is of 5 mm in dimension, the TPS based method seems adequate to correlate the functional data onto the corresponding voxels in CT.

In order to examine the consistency of the registration, we inverted the previous transformation procedure by transforming the TPS-warped images [Figs. 3(B)–3(D) middle panels] back to the distorted *floating* images. The calculation results are shown in the left columns of Figs. 4(A)–4(C). The original deformed phantom images (the left columns of Fig. 3) are subtracted from them and are shown in the right panels. The resultant overlap of fiducial points was excellent in all three cases, suggesting the TPS is capable of generating consistent good mapping independent of the starting images. The MLDEs for the three groups were 0.23±0.08, 0.23±0.18, and 0.20±0.11 mm, respectively. Maximum landmark registration discrepancies were found to be 0.35, 0.50, and 0.31 mm, respectively [Fig. 4(D)].

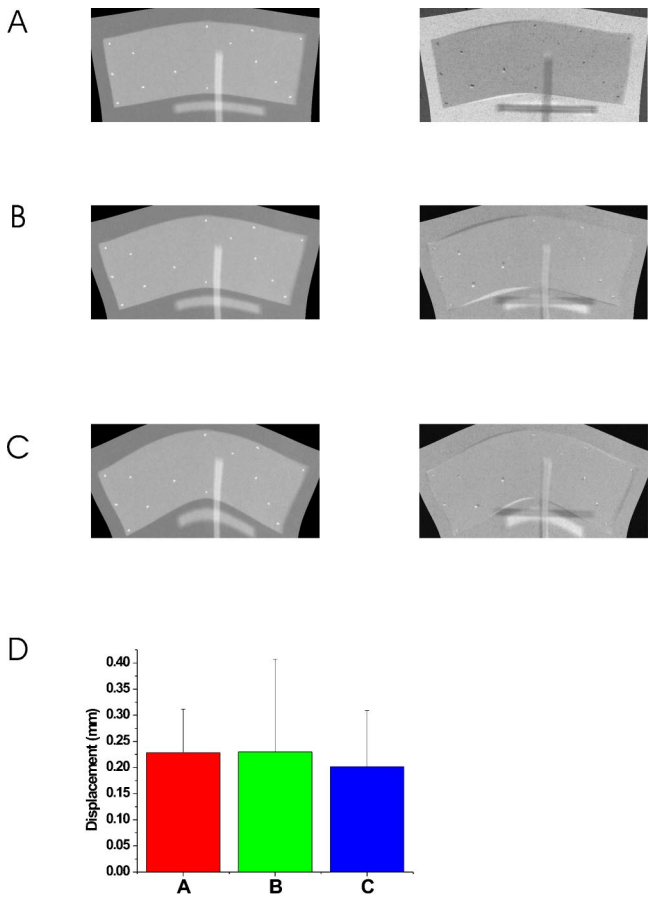

FIG. 4. Registration consistency test. Left panels of (A), (B), and (C) represent the computer-warped images with the middle panel images of Figs. 3(B)–3(D) as input. Right panels of (A), (B), and (C) represent the corresponding difference images between the mapped and the original images. (D), Landmark displacement between the model prediction and the actual position for the three groups.

B. Patient studies

We first studied where the distortion most likely happens in the ER-based MR images. After target segmentation and rotation operation, we compared the dimensions of the prostate in the datasets of three patients. The height of the prostate along superior-posterior axis was found almost the same (3.1% discrepancy) in CT and ER based-MR images. The width along left-right axis and the length along anterior–posterior axis differ a lot between CT and MR images. We measured the width and length of the prostate in the middle axial slices of three patients. The width of the prostate in MRI is (115.0±1.7)% of that of the prostate in CT. The length of the prostate in MRI is (83.3±1.5)% of that of the prostate in CT. After further comparing the shape of the prostates in CT and ER-MRI, we conclude that distortion mostly happens in the transverse plane. This observation suggests that, to a reasonable approximation, we could perform the mapping procedure in a slice by slice fashion.

The TPS transformation was applied to the coregistration of the CT and ER-based MR images. We show a representative axial slice of a patient's CT images in Fig. 5(A). To have a better view of the volume of interest, we selected a rectangular region encompassing the prostate [Fig. 5(A) right]. The MR images were acquired with high resolution and the posterior portion of the image was distorted by the presence of the ER coil [Fig. 5(B) left]. Eight control points were chosen along the contour of the corresponding MR and CT images. TPS transformation was applied to the distorted MR image and the mapped MRI contour of the prostate overlapped almost completely with that from the CT scan [Fig. 5(B) right]. Difference between TPS-derived MR contour and CT contour is shown in Fig. 5(C). Most prostate regions were in good agreement including the seriously contorted left and right posterior regions of the image. Similar results were obtained from the other patient.

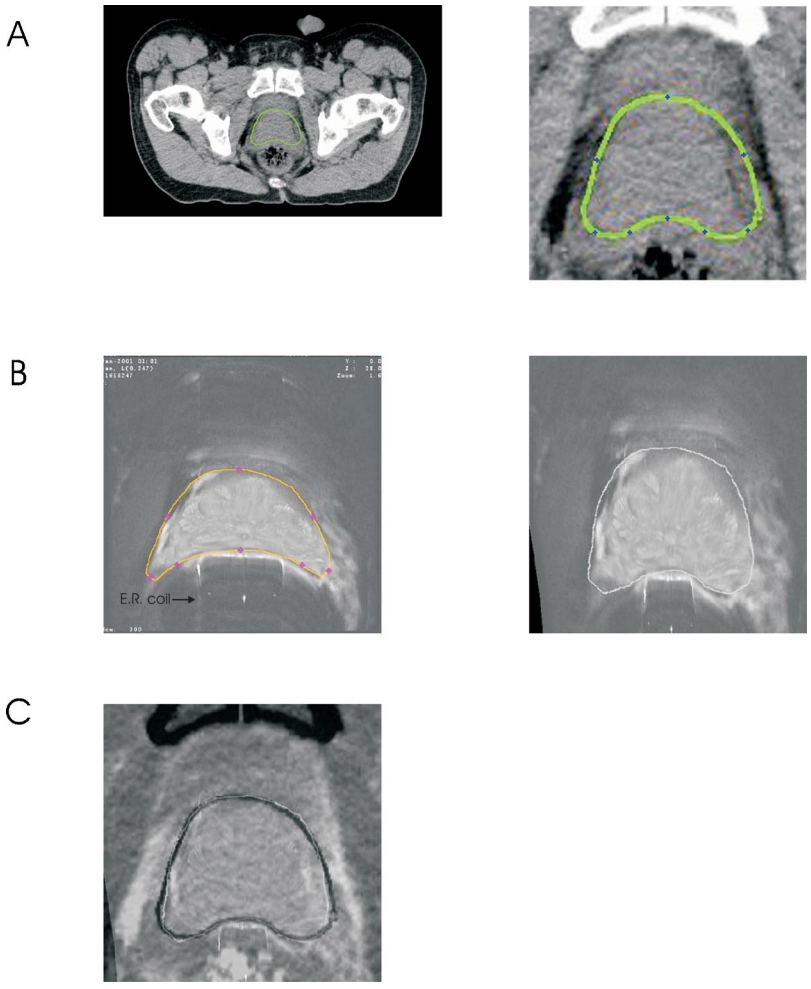

FIG. 5. Deformable registration of the prostate gland in a patient. (A) A transverse CT study (left) and a region of interest encompassing the prostate (right). The control points are denoted with plus signs. (B) The MRI study (left) and transformed image (right) by TPS based registration. The control points are denoted with plus signs. (C) Difference between the CT and the mapped MR image.

We used centroid position displacement and coincidence index (CI) between the mapped MR images and the CT images to quantify the registration accuracy for three datasets. Using the TPS method, the centroid displacement was 0.56 ± 0.09 mm, significantly less than that of the nondeformable registration [2.03 ± 0.38 mm, Fig. 6(A)]. The CI indices were found to be close to unity $(93.1 \pm 5.0)\%$, indicating that the TPS algorithm is able to model the nonrigid soft tissue deformation caused by the endorectal coil placement [Fig. 6(B)]. On the other hand, a much lower CI, $(49.5 \pm 8.9)\%$, was found when using the nondeformable registration. This suggests that fusion with a rigid-body transformation and scaling is inadequate to deal with the system involving the images acquired with the ER coils.

The registration error depends on the appropriate placement of control points. We studied registration inconsistencies between different trials of one operator and between three operators. The intraoperator experiment was repeated five times on one patient's data. The centroid displacement was found to be in the range of 0.31–0.65 mm. The CI indices were found to be from 91.7% to 93.5%. Three operators were asked to repeat the control point placement five times and the mean results between the operators were compared. The centroid displacements were found to be 0.55 ± 0.30, 0.47 ± 0.17, and 0.54 ± 0.25 mm, respectively. The CI indices, corresponding to three operators, were $(92.7 \pm 0.9)\%$, $(93.5 \pm 0.7)\%$, and $(92.5 \pm 1.2)\%$, respectively. The centroid displacement and CI index show no significant difference between trials and operators.

IV. DISCUSSION AND CONCLUSION

Registration has been implemented in several commercial medical image analysis and radiation treatment planning systems. For example, Radionics (Radionics™, Burlington, MA) has developed ImageFusion software which provides the ability to fuse multiple image sets based on the mutual information. AcQSim Oncodiagnostic Simulation/Localization System (Philips Medical Systems, Cleveland, OH) provides two registration methods: point matching (a minimum of three common points need to be selected on both sets of images registered) and interactive image-based registration (a color wash of one image set is displayed over a gray scale image of the other). At this point, they all use a rigid-body transformation and scaling, which maintain the straightness of lines, and hence cannot accommodate contour/shape distortion. In reality, the shape of the prostate gland can be easily changed by many factors such as patient position change, invasive brachytherapy procedures or endorectal coil placement during high resolution MR/MRS im-

ages acquisition.[28] To help physicians to segment the prostate gland and possible intraprostatic lesions by incorporating MRI/MRSI metabolic data on a CT-based treatment planning system, there is an indisputable need for developing a computationally efficient deformable registration technique to achieve voxel to voxel mapping. In this work, we used a TPS method to register the endorectal coil-based MR data with CT images. The data presented in the last section suggests that the TPS technique is well suited for this type of application.

The warping process was carried out in a 2D slice-by-slice and is worthy of further investigation. This may result in the registration error in the longitudinal direction. Based on our observations for the three patients involved in this study, it seems that the distortion occurs mainly along the right–left and the anterior–posterior directions. The height of the prostate along the superior–inferior axis changes insignificantly in the MR and CT datasets. This is consistent with the finding by another group in 1.5 T MR imaging of the prostate.[28] In actuality, it is possible to extend the current quasi-3D model to a fully 3D one. The current study sheds useful insight into this type of extension and provides a natural starting point for the implementation of a complete 3D TPS mapping. We are aware that the prostate volume drawn from CT may be different from that in MR.[29] Currently we simply rely on the expert opinions from the radiation oncologist. Hopefully, with the common efforts from physicists and physicians, this difficult issue will be resolved in the near future.

A few more sophisticated deformable registration methods have been investigated by several groups. A viscous-fluid transformation and fluid-landmark registration technique have been proposed to model the nonrigid deformation of organs in intracavitary brachytherapy.[27,30] A finite-element method has been used to model the tissue mechanical property and to register brain and prostate images.[31,32] A biomechanical model of an elastic body has been used to quantify patient organ motion in the process of radiation therapy so that the dose delivered on the volume of a deforming organ can be accumulated.[33] These methods are usually computationally intensive. Moreover, the model parameters normally need to be determined empirically because of the lack of tissue biomechanical data in the literature, which compromises the advantages of these physics-based models. More recently, some registration schemes are designed to match both control point and intensity information.[34–36] In addition to guaranteeing a one to one correspondence of the prescribed control points, they minimize an intensity based measure for the remaining parts of the images. The method should yield higher accuracy than the control point only based method and should be more computationally efficient than the intensity only based method. In addition to computation efficiency, there are another two considerations for us to use the TPS based registration. Firstly, our ultimate goal is to map the metabolic data of MRSI to the correct voxels in CT. The voxel size of MRSI is generally very coarse (currently ~5 mm) compared to the anatomic images. The increased registration accuracy by more advanced methods may be not necessary for this mapping purpose. Secondly, our registration target is the prostate only which is of similar intensity. The linear interpolation after matching control points in TPS should be sufficiently accurate for registering a uniform small structure. The phantom and patient studies have shown that the TPS approach is computationally efficient and can yield clinically acceptable registration accuracy for our purpose.

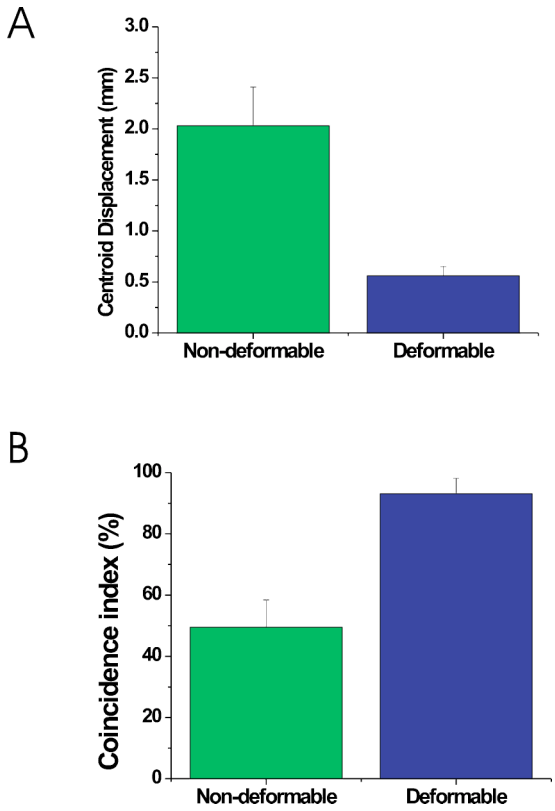

FIG. 6. Centroid position displacement (A) and coincidence index of deformable and nondeformable registration in patient studies (B).

It is noted that the TPS based registration needs manual placement of control points, which requires the input from an experienced clinician. This is similar to the previously reported rigid body-based registration method.[17,21] The intra- and interoperator experiments have shown that the variances of results are small and registration accuracy does not depend on the different operators or different trials significantly.

In conclusion, we have implemented a TPS transformation algorithm to map voxels in endorectal coil-based prostate MR/MRS images with those in CT images. The deformable mapping technique significantly improved the previously reported nondeformable method and should be adequate for routine clinical application. The accuracy of the approach has been tested by using phantom and patient studies. The registration scheme should be useful to map the functional MRSI data onto CT to guide the design of conformal radiation treatment plans.

ACKNOWLEDGMENTS

This work was presented in the 45th ASTRO annual meeting in 2003. We would like to thank the assistance of A.

Boyer, C. Cardenas, F. van den Haak, and Y. Yang from Stanford University. We also appreciate the enlightening discussions with S. Chang and L. Goyal from The University of North Carolina at Chapel Hill, and W. Du from The University of Chicago. This work was in part supported by a research grant from the prostate cancer research program of U.S. Department of Defense (DAMD17-03-1-0023).

[a]Present address: Department of Radiation Oncology, The University of North Carolina, 101 Manning Dr., Chapel Hill, North Carolina 27599-7512. E-mail: Jun_Lian@med.unc.edu; Phone: (919) 966 1101; Fax: (919) 966 7681.

[b]Author to whom correspondence should be addressed. E-mail: lei@reyes.stanford.edu; Phone: (650) 498 7896; Fax: (650) 498 4015.

[1]C. Bartolozzi, L. Crocetti, I. Menchi, S. Ortori, and R. Lencioni, "Endorectal magnetic resonance imaging in local staging of prostate carcinoma," Abdom. Imaging **26**, 111–122 (2001).

[2]M.D. Schnall, Y. Imai, J. Tomaszewski, H.M. Pollack, R.E. Lenkinski, and H.Y. Kressel, "Prostate cancer: Local staging with endorectal surface coil MR imaging," Radiology **178**, 797–802 (1991).

[3]M.D. Schnall, R.E. Lenkinski, H.M. Pollack, Y. Imai, and H.Y. Kressel, "Prostate: MR imaging with an endorectal surface coil," Radiology **172**, 570–574 (1989).

[4]J.F. Martin, P. Hajek, L. Baker, V. Gylys-Morin, R. Fitzmorris-Glass, and R.R. Mattrey, "Inflatable surface coil for MR imaging of the prostate," Radiology **167**, 268–270 (1988).

[5]R.A. Huch Boni, C. Meyenberger, J. Pok Lundquist, F. Trinkler, U. Lutolf, and G.P. Krestin, "Value of endorectal coil versus body coil MRI for diagnosis of recurrent pelvic malignancies," Abdom. Imaging **21**, 345–352 (1996).

[6]Y. Kaji, J. Kurhanewicz, H. Hricak, D.L. Sokolov, L.R. Huang, S.J. Nelson, and D.B. Vigneron, "Localizing prostate cancer in the presence of postbiopsy changes on MR images: Role of proton MR spectroscopic imaging," Radiology **206**, 785–790 (1998).

[7]J. Kurhanewicz, D.B. Vigneron, H. Hricak, P. Narayan, P. Carroll, and S.J. Nelson, "Three-dimensional H-1 MR spectroscopic imaging of the *in situ* human prostate with high (0.24-0.7-cm^3) spatial resolution," Radiology **198**, 795–805 (1996).

[8]L. Kwock, J.K. Smith, M. Castillo, M.G. Ewend, S. Cush, T. Hensing, M. Varia, D. Morris, and T.W. Bouldin, "Clinical applications of proton MR spectroscopy in oncology," Technol. Cancer Res. Treatment **1**, 17–28 (2002).

[9]J.C. Presti, Jr., H. Hricak, P.A. Narayan, K. Shinohara, S. White, and P.R. Carroll, "Local staging of prostatic carcinoma: comparison of transrectal sonography and endorectal MR imaging," AJR, Am. J. Roentgenol. **166**, 103–108 (1996).

[10]H. Hricak, G.C. Dooms, R.B. Jeffrey, A. Avallone, D. Jacobs, W.K. Benton, P. Narayan, and E.A. Tanagho, "Prostatic carcinoma: Staging by clinical assessment, CT, and MR imaging," Radiology **162**, 331–336 (1987).

[11]M. Perrotti, R.P. Kaufman, Jr., T.A. Jennings, H.T. Thaler, S.M. Soloway, M.D. Rifkin, and H.A. Fisher, "Endo-rectal coil magnetic resonance imaging in clinically localized prostate cancer: Is it accurate?," J. Urol. (Baltimore) **156**, 106–109 (1996).

[12]G.J. Jager, J.L. Severens, J.R. Thornbury, J.J. de La Rosette, S.H. Ruijs, and J.O. Barentsz, "Prostate cancer staging: Should MR imaging be used?—A decision analytic approach," Radiology **215**, 445–451 (2000).

[13]S.F. Quinn, D.A. Franzini, T.A. Demlow, D.R. Rosencrantz, J. Kim, R.M. Hanna, and J. Szumowski, "MR imaging of prostate cancer with an endorectal surface coil technique: correlation with whole-mount specimens," Radiology **190**, 323–327 (1994).

[14]P. Xia, B. Pickett, E. Vigneault, L.J. Verhey, and M. Roach, 3rd, "Forward or inversely planned segmental multileaf collimator IMRT and sequential tomotherapy to treat multiple dominant intraprostatic lesions of prostate cancer to 90 Gy," Int. J. Radiat. Oncol., Biol., Phys. **51**, 244–254 (2001).

[15]S.J. DiBiase, K. Hosseinzadeh, R.P. Gullapalli, S.C. Jacobs, M.J. Naslund, G.N. Sklar, R.B. Alexander, and C. Yu, "Magnetic resonance spectroscopic imaging-guided brachytherapy for localized prostate cancer," Int. J. Radiat. Oncol., Biol., Phys. **52**, 429–438 (2002).

[16]L. Xing, C. Cotrutz, S. Hunjan, A.L. Boyer, E. Adalsteinsson, and D. Spielman, "Inverse planning for functional image-guided intensity-modulated radiation therapy," Phys. Med. Biol. **47**, 3567–3578 (2002).

[17]M. Zaider, M.J. Zelefsky, E.K. Lee, K.L. Zakian, H.I. Amols, J. Dyke, G. Cohen, Y. Hu, A.K. Endi, C. Chui, and J.A. Koutcher, "Treatment planning for prostate implants using magnetic-resonance spectroscopy imaging," Int. J. Radiat. Oncol., Biol., Phys. **47**, 1085–1096 (2000).

[18]C.C. Ling, J. Humm, S. Larson, H. Amols, Z. Fuks, S. Leibel, and J.A. Koutcher, "Towards multidimensional radiotherapy (MD-CRT): Biological imaging and biological conformality," Int. J. Radiat. Oncol., Biol., Phys. **47**, 551–560 (2000).

[19]J. Lian, S. Hunjan, C. Dumoulin, J. Levin, R. Watkins, K. Rohling, R. Giaquinto, D. Kim, A. Lo, D. Spielman, B. Daniel, and L. Xing, "Integrating deformable MRI/MRSI and CT image registration into the prostate IMRT treatment planning," Int. J. Radiat. Oncol., Biol., Phys. **57**, S207 (2003).

[20]X. Wu, C.X. Yu, S.J. DiBiasea, and R. Gullapallib, "The application of deformable image registration for MRS in prostate treatment planning," Int. J. Radiat. Oncol., Biol., Phys. **57**, S207–S208 (2003).

[21]T. Mizowaki, G.N. Cohen, A.Y. Fung, and M. Zaider, "Towards integrating functional imaging in the treatment of prostate cancer with radiation: The registration of the MR spectroscopy imaging to ultrasound/CT images and its implementation in treatment planning," Int. J. Radiat. Oncol., Biol., Phys. **54**, 1558–1564 (2002).

[22]B. Fei, A. Wheaton, Z. Lee, J.L. Duerk, and D.L. Wilson, "Automatic MR volume registration and its evaluation for the pelvis and prostate," Phys. Med. Biol. **47**, 823–838 (2002).

[23]B. Fei, C. Kemper, and D.L. Wilson, "A comparative study of warping and rigid body registration for the prostate and pelvic MR volumes," Comput. Med. Imaging Graph. **27**, 267–281 (2003).

[24]K.M. Brock, J.M. Balter, L.A. Dawson, M.L. Kessler, and C.R. Meyer, "Automated generation of a four-dimensional model of the liver using warping and mutual information," Med. Phys. **30**, 1128–1133 (2003).

[25]S. Fantozzi, A. Cappello, and A. Leardini, "A global method based on thin-plate splines for correction of geometric distortion: An application to fluoroscopic images," Med. Phys. **30**, 124–131 (2003).

[26]F.L. Bookstein, "Principal Warps: Thin Plate Splines and the Decomposition of Deformations," IEEE Trans. Pattern Anal. Mach. Intell. **11**, 567–585 (1989).

[27]G.E. Christensen, B. Carlson, K.S. Chao, P. Yin, P.W. Grigsby, K. Nguyen, J.F. Dempsey, F.A. Lerma, K.T. Bae, M.W. Vannier, and J.F. Williamson, "Image-based dose planning of intracavitary brachytherapy: Registration of serial-imaging studies using deformable anatomic templates," Int. J. Radiat. Oncol., Biol., Phys. **51**, 227–243 (2001).

[28]M. Hirose, A. Bharatha, N. Hata, K.H. Zou, S.K. Warfield, R.A. Cormack, A. D'Amico, R. Kikinis, F.A. Jolesz, and C.M. Tempany, "Quantitative MR imaging assessment of prostate gland deformation before and during MR imaging-guided brachytherapy," Acad. Radiol. **9**, 906–912 (2002).

[29]C. Rasch, I. Barillot, P. Remeijer, A. Touw, M. van Herk, and J.V. Lebesque, "Definition of the prostate in CT and MRI: A multiobserver study," Int. J. Radiat. Oncol., Biol., Phys. **43**, 57–66 (1999).

[30]S.C. Joshi and M.I. Miller, "Landmark matching via large deformation diffeomorphisms," IEEE Trans. Image Process. **9**, 1357–1370 (2000).

[31]A. Bharatha, M. Hirose, N. Hata, S.K. Warfield, M. Ferrant, K.H. Zou, E. Suarez-Santana, J. Ruiz-Alzola, A. D'Amico, R.A. Cormack, R. Kikinis, F.A. Jolesz, and C.M. Tempany, "Evaluation of three-dimensional finite element-based deformable registration of pre- and intraoperative prostate imaging," Med. Phys. **28**, 2551–2560 (2001).

[32]M. Ferrant, A. Nabavi, B. Macq, F.A. Jolesz, R. Kikinis, and S.K. Warfield, "Registration of 3-D intraoperative MR images of the brain using a finite-element biomechanical model," IEEE Trans. Med. Imaging **20**, 1384–1397 (2001).

[33]D. Yan, D.A. Jaffray, and J.W. Wong, "A model to accumulate fractionated dose in a deforming organ," Int. J. Radiat. Oncol., Biol., Phys. **44**, 665–675 (1999).

[34]B. Fischer and J. Modersitzki, *Intensity Based Image Registration With a Guaranteed One-to-One Point Match*, Advances in Biomedical Image Analysis, Selected Papers from the German BVM-Workshop on Medical Image Processing, Special Issue, Methods of Information in Medicine, edited by T. Tolxdorff (Schattauer Verlag, Stuttgart, 2003).

[35]A. Fischer and J. Modersitzki, "Combining landmark and intensity driven registrations," PAMM **3**, 32–35 (2003).

[36]J. Kybic and M. Unser, "Fast parametric elastic image registration," IEEE Trans. Image Process. **12**, 1427–1442 (2003).